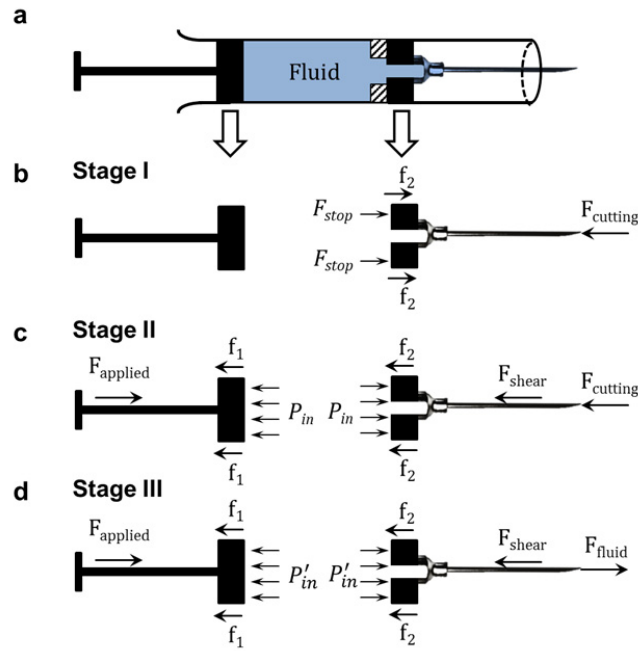


Table of Contents

S1. Needle motion analysis	2
Supplementary figure S1-1	2
Supplementary figure S1-2	6
S2. Micro CT images at multiple pressures	7
Supplementary figure S2.....	7
S3. Intravitreal injection using standard 30 G needle	8
Supplementary figure S3.....	8
S4. Serial sections along the path of the needle targeting SCS	9
Supplementary figure S4.....	9
S5. Variability in dead volume can be reduced by decreasing the diameter of needle plunger	11
Supplementary figure S5.....	11
S6. Use of i2T2 in other tissue types and its potential applications	12
Supplementary figure S6.....	12
Caption for Supplementary video 1	13
Caption for Supplementary video 2	13

S1. Needle motion analysis:

To study this behavior and predict the design specifications that enable the *i2T2* mechanism, we developed an analytical model of the device. The overall process of injecting with the auto-stop syringe can be divided into three distinct stages, stage I to III (supplementary figure S1-1). In stage I, the needle is inserted into the superficial tissue, where the tissue serves as a fluidic resistance to block the fluid flow. In stage II the operator starts applying force to the pushing-plunger to advance the needle through the tissue. As the needle tip reaches in tissue interface or cavity, it automatically stops even if the operator continues to push on the plunger. In stage III the needle is idle, while the operator continues to push on the plunger, fluid is delivered to the tissue interface or cavity.



Supplementary figure S1-1: Force diagram of *i2T2* (a) schematic (b) stage I (c) stage II and (d) stage III

Stage I: Pre-insertion of the needle:

During stage I, i.e. pre-insertion, the needle tip cuts through the tissue and becomes buried in the tissue. This creates a large resistance for the fluid to escape through the needle tip critical to enable needle motion in stage II (see below). During the process of pre-insertion, the needle experiences a backward force by the tissue. This force is nullified by the normal force applied by the mechanical stop designed to avoid a backward motion of the needle relative to the syringe. Based on the force body diagram (figure 1a),

$$F_{\text{stop}} + f_2 = F_{\text{Cutting}} \quad (1)$$

Where,

F_{stop} : Normal force applied by the needle plunger seat on the plunger

f_2 : Frictional forces between the rubber seals on needle and barrel wall

F_{cutting} : Cutting force at the tip

In the absence of a needle-plunger seat, frictional force may not be sufficient to keep the needle from moving relative to the syringe barrel. If the needle starts moving backward, it would pressurize the inner fluid and the fluid would start exiting the needle. To avoid unwanted release before tissue insertion, a mechanical stop is designed in such a manner that it provides sufficient normal force to enable pre-insertion in the tissue without pressurizing the internal fluid.

Stage II: Needle motion through the bulk tissue

In stage II the needle pierces through the tissue wall as the user pushes on the pushing-plunger. The needle motion is enabled by raised internal pressure as the user applies force on the pushing-plunger. Assuming a quasistatic process and negligible infusion into the tissue, we can write the force balance equations as (supplementary figure 1b),

$$P_{in} * A_2 = f_2 + F_{Cutting} + F_{shear} \quad (2)$$

$$F_{applied} = P_{in} * A_1 + f_1 \quad (3)$$

Where,

P_{in} : Internal fluid pressure

A_1 : Internal area of the pushing plunger

A_2 : Internal area of the needle support

F_{shear} : Shear force applied by surrounding tissue on the needle

$F_{cutting}$: Cutting force at the tip

f_1 : Frictional forces between the rubber seals on the pushing plunger and barrel wall.

f_2 : Frictional forces between the rubber seals on needle support and barrel wall.

$F_{applied}$: External force applied on the pushing plunger

Hence the needle will move through the tissue if,

$$\text{Driving force} = P_{in} * A_2 > f_2 + F_{Cutting} + F_{shear} = \text{Opposing force} \quad (4)$$

OR

$$\text{Driving force}_{min} = (P_{in})_{min} * A_2 = f_2 + F_{Cutting} + F_{shear} = \text{Opposing force} \quad (5)$$

i.e. the needle will move through the tissue, only if the seal created by tissue during pre-insertion can withstand a pressure of $(P_{in})_{min}$ or higher.

We experimentally measured the opposing force ($f_2 + F_{Cutting} + F_{shear}$) for a range of syringes and needles for bovine sclera using a mechanical tester (fig 3 e and f). Fresh scleral tissue was mounted on a holder to hold it taut, and the needle mounted on the needle plunger was pre-inserted into the tissue and pushed through the tissue at a given speed while continuously measuring the opposing force. In this manner we measured the collective opposing force for a single setting instead of performing three separate measurements for each force. Considering visco-elastic behavior of scleral tissue, we performed measurements at multiple speeds. These opposing forces are plotted in figure 3a.

The internal pressure (P_{in}), which controls the driving force, is directly proportional to the applied force. For large opposing force, one may increase the applied force, however, there is a limit on the internal pressure, beyond which the seal created by the tissue will not hold. Therefore, we have an upper limit of the driving force, which is determined by tissue's resistance to fluid-flow. When the fluid-flow-rate through the leaky tissue-seal equals the flow-rate determined by the speed of pushing plunger, the needle-plunger will remain stationary and needle will not advance through the tissue. We measured this maximum allowable driving force for a range of syringes and needles for bovine sclera using a mechanical tester. For measurements, the needle was pre-inserted into a taut (stretched) bovine sclera mounted on a holder. This needle was mounted on a standard syringe which was clamped to hold the position. Then the plunger was pushed at a given speed to generate fluid flow while the needle tip was

sealed by the tissue and applied force on the plunger was monitored continuously. Frictional force (measured separately) was subtracted from the measurements to obtain the maximum allowable driving force. Measurements were performed at a range of fluid-flow-rates by changing the speed of pushing-plunger. These values are plotted in figure 3a along with opposing force. Driving force higher than opposing force indicates that the needle will move through the tissue.

Stage III: Arrested needle motion in the cavity.

At the end of stage II, the needle tip enters the cavity, where resistance to the fluid to flow out of the needle suddenly drops. This is stage III where a new force equilibrium is established (supplementary figure 1d). Accordingly, force balance equations are,

$$F_{\text{applied}} = P'_{\text{in}} * A_1 + f_1 \quad (6)$$

$$P'_{\text{in}} * A_2 + F_{\text{fluid drag}} = f_2 + F_{\text{shear}} \quad (7)$$

Where,

P'_{in} : Stage III internal fluid pressure

A_1 : Internal area of the pushing plunger

A_2 : Internal area of the needle support

F_{shear} : Shear force applied by surrounding tissue on the needle

f_1 : Frictional forces between the rubber seals on the pushing plunger and barrel wall

f_2 : Frictional forces between the rubber seals on needle plunger and barrel wall

F_{applied} : External force applied on the pushing plunger

$F_{\text{fluid drag}}$ = drag force applied by the fluid flowing inside the needle

Hence for the needle to stop at the interface, we need

$$P'_{\text{in}} * A_2 + F_{\text{fluid drag}} < f_{2_max} + F_{\text{shear}} \quad (8)$$

OR

$$(P'_{\text{in}})_{\text{max}} * A_2 + (F_{\text{fluid drag}})_{\text{max}} = f_{2_max} + F_{\text{shear}} \quad (9)$$

Where

$(P'_{\text{in}})_{\text{max}}$ = maximum internal pressure that allow the needle to remain stationary

f_{2_max} = maximum static friction offered by the needle plunger

$(F_{\text{fluid}})_{\text{max}}$ = maximum drag force applied by the fluid flowing inside the needle as a function of flow rate.

Considering that the force applied by the tissue (F_{shear}) can vary based on tissue type, we can apply a more stringent condition for design requirements, to eliminate dependency on the tissue type.

$$(P'_{\text{in}})_{\text{design}} * A_2 + (F_{\text{fluid drag}})_{\text{design}} = f_2 < f_2 + F_{\text{shear}} \quad (9)$$

Hence as long as the internal pressure and fluid drag force do not overcome frictional forces, the needle will stop at the interface. Similar to stage II we can collectively term these forces as driving and opposing forces:

$$\text{Driving force} = (P'_{\text{in}})_{\text{design}} * A_2 + (F_{\text{fluid drag}})_{\text{design}} \quad (10)$$

$$\text{Opposing force} = f_2 \quad (11)$$

We experimentally measured the driving force by pushing the fluid through a range of needles and syringes at multiple flow rates. The needle was mounted on a clamped syringe and a plunger was pushed

at varying speeds while fluid was allowed to flow through the needle tip freely and while measuring the applied force. Frictional force of the plunger (measured separately) was subtracted from the measurements to obtain the total driving force. Opposing force, i.e. frictional force by the needle plunger was measured with a mechanical tester. These experimental measurements of driving and opposing forces are plotted in figure 2b.

To extend the understanding of the system and predict functionality beyond the experimental measurement, we modeled the system in Mathematica based on empirically-determined frictional forces and theoretical fluid mechanics to establish correlations that predict successful delivery of the fluid in the cavity.

Based on Hagen-Poiseuille equation,

$$P'_{in} = \frac{128\mu LQ}{\pi d^4} \quad (12)$$

For a circular pipe drag force by fluid on the pipe can be expressed as,

$$F_{fluid\ drag} = \frac{8\pi\mu LQ}{A_{Needle}} \quad (13)$$

Where,

μ =Fluid viscosity

L = Needle length

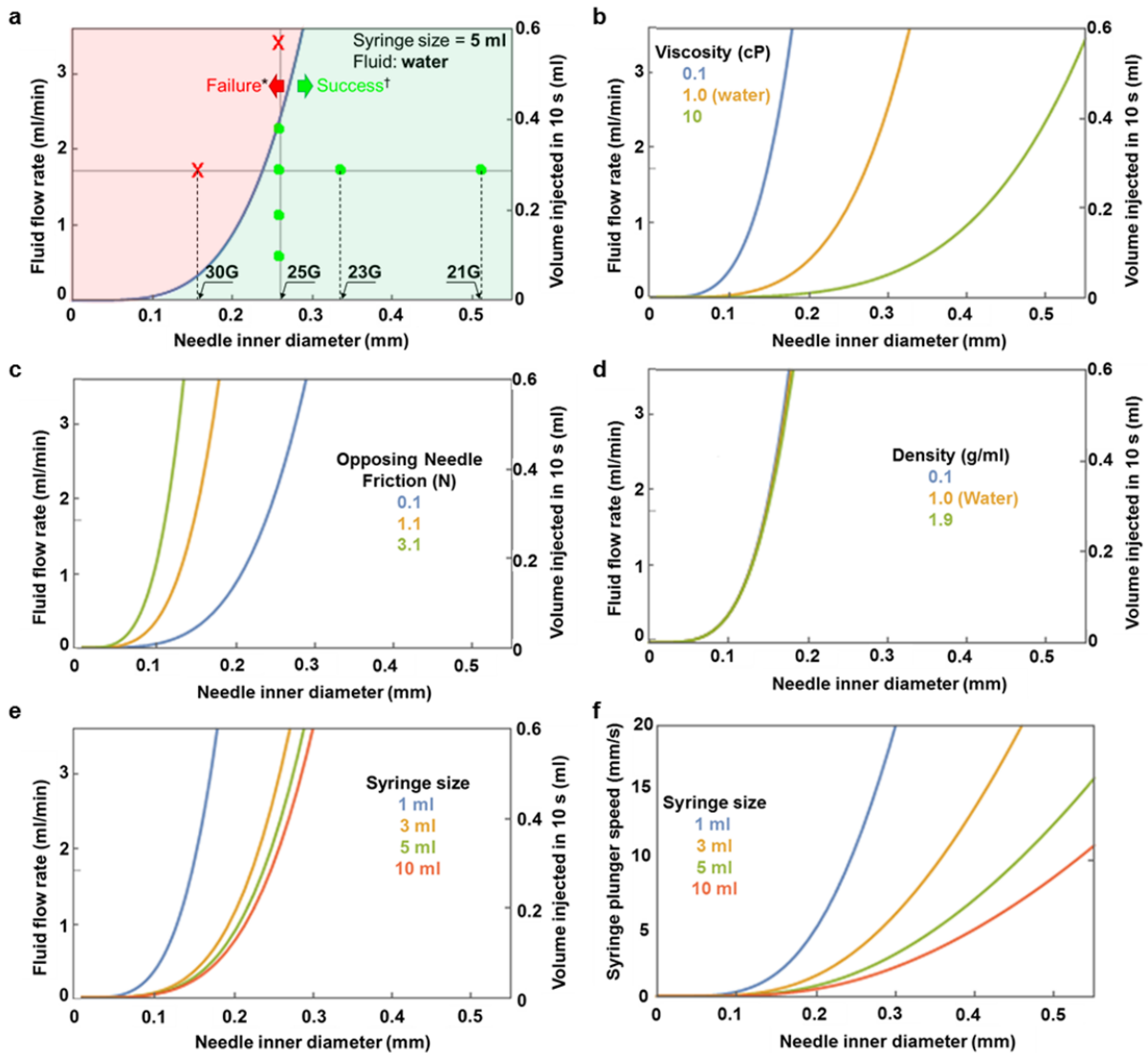
Q = Fluid flow rate (=V*A)

d = Needle inner diameter

A_{Needle} = Inner cross-sectional area of needle

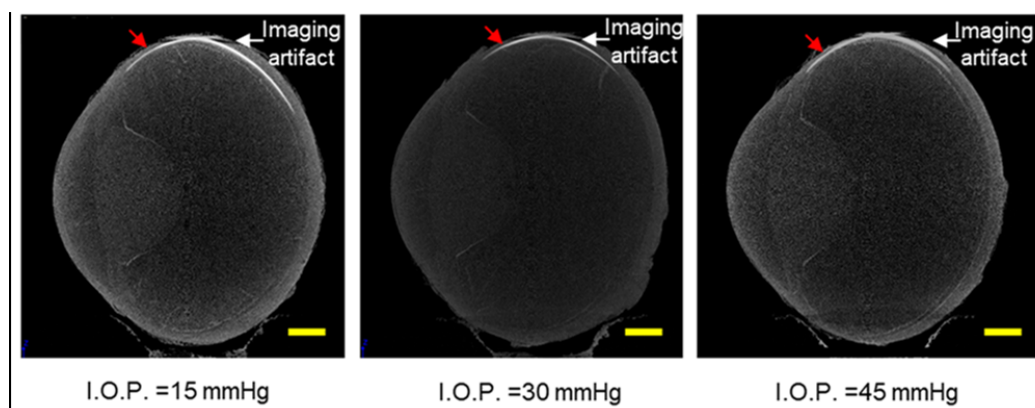
Substituting these into the stage III force condition mentioned earlier (Eq. 9), yields a correlation between needle size, syringe size, fluid viscosity, fluid flow rate. These equations were solved using Mathematica and plotted for a range of threshold flow rate values. This analysis revealed a threshold flow rate for each combination of needle size, syringe size, fluid viscosity, and frictional coefficients, beyond which the needle will advance despite reaching the cavity. Clinically, this implies that injecting too fast can cause needle overshoot and inject drug into vitreous instead of SCS. The threshold flow rate increases non-linearly as a function of needle inner diameter (Supp. fig. 1-2c). Modeled results of the threshold are validated by testing multiple combinations of needle size and flow rate. This analytical model has enabled us to predict the effect of viscosity (Supp. fig. 1-2d), syringe size (Supp. fig. 1-2e) and frictional coefficient (Supp. fig. 1-2f) on the threshold flow rate.

The analytical model developed for design decisions, assumes a formulation comprising an incompressible, Newtonian fluid, such as water and aqueous formulations commonly used for ocular injections. Non-Newtonian fluids – compressible (i.e., gases) or shear thinning fluids (i.e., hyaluronic acid) – can directly impact needle motion. Adapting the model to accommodate such fluids can help to modify the device corresponding applications. Regardless of the formulation's fluid properties, one can gain access to the SCS by first injecting a neutral fluid (e.g. saline) through the i2T2, followed by injecting the formulation of interest.



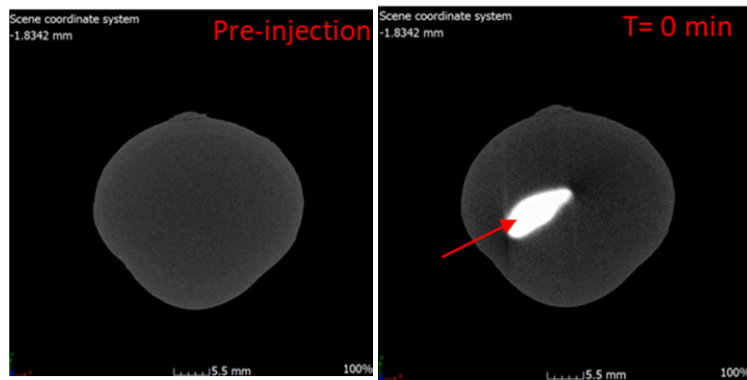
Supplementary figure S1-2: (a) Threshold flowrate plot for water with 5 ml syringe, data points indicate experimental outcomes. (* Failure indicates forward movement of needle while fluid is flowing through the tip and †success indicates idle needle as fluid flows through the tip) (b) Increasing viscosity of the formulation shifts the threshold flowrate plot indicating larger needles would be needed. (c) Increasing opposing friction enables one to use smaller needles at higher flow rate (d) Density of the formulation has minimal impact on the system. (e-f) Change in syringe size changes the frictional force and cross-sectional area of the plungers, directly influencing the threshold flow rate. This effect is also dependent on the syringe/needle design. (e) Shows the threshold flow rates for the design depicted in Fig. 1(h) and (f) shows that for the design in Fig. 1k.

S2. Micro CT images at multiple pressures



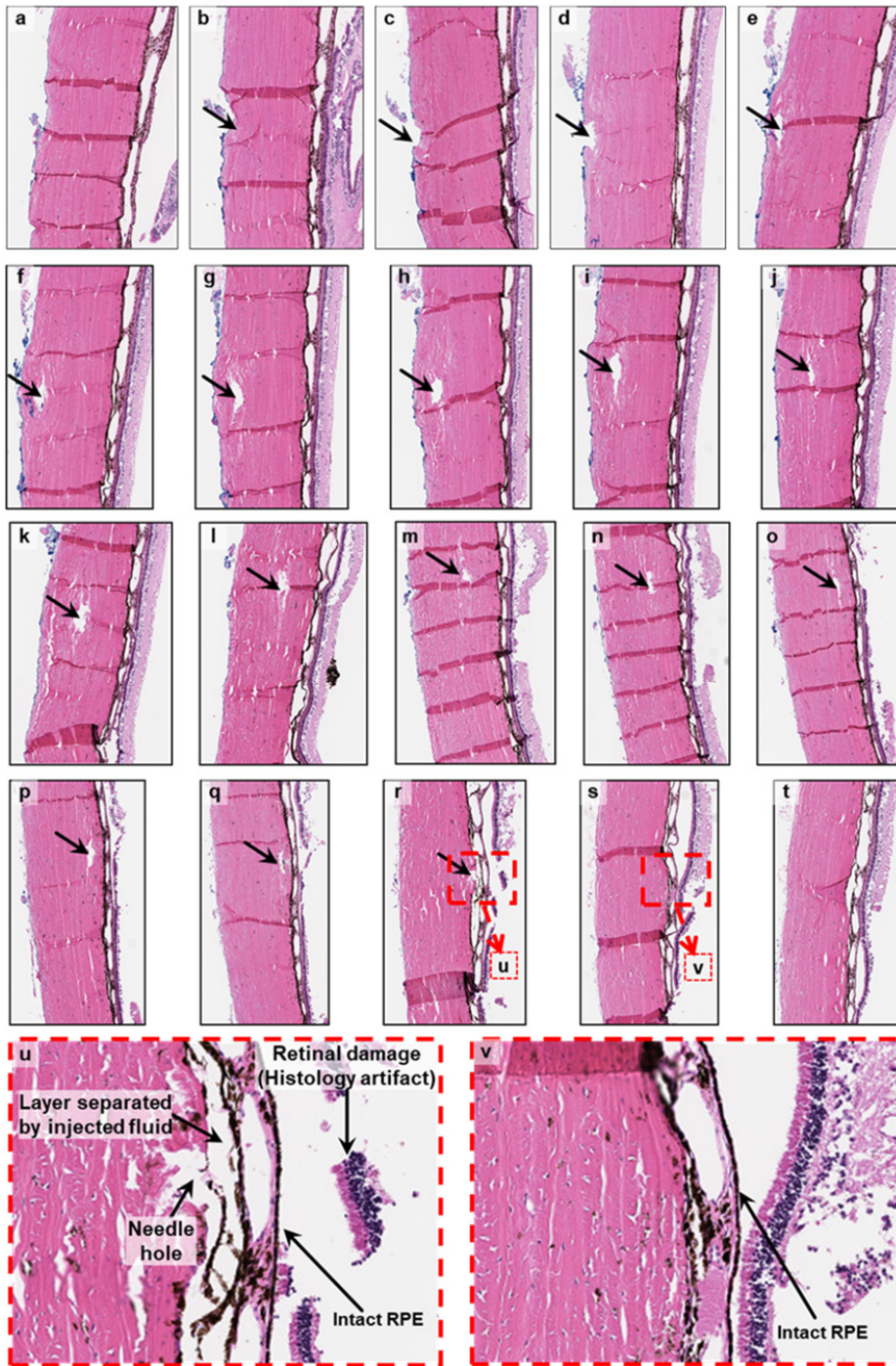
Supplementary figure S2: MicroCT cross-section images of bovine eyes injected with Ultravist™ contrast agent (diluted with P.B.S. 1:1, 150 μ l) at multiple I.O.P.s. Injected contrast agent disperses along periphery to reach the back of the eye. Red arrow shows the approximate position of needle insertion. White arrow points to the black stripe on sclera which is an imaging artifact. Samples were frozen immediately after injection and frozen tissue was imaged with microCT. The experiments were repeated independently (n=3) with similar results.

S3. Intravitreal injection using standard 30 G needle



Supplementary figure S3: MicroCT image of a bovine eye after performing an intravitreal injection ex vivo. The arrow indicates the injected contrast agent. The experiments were repeated independently (n=3) with similar results.

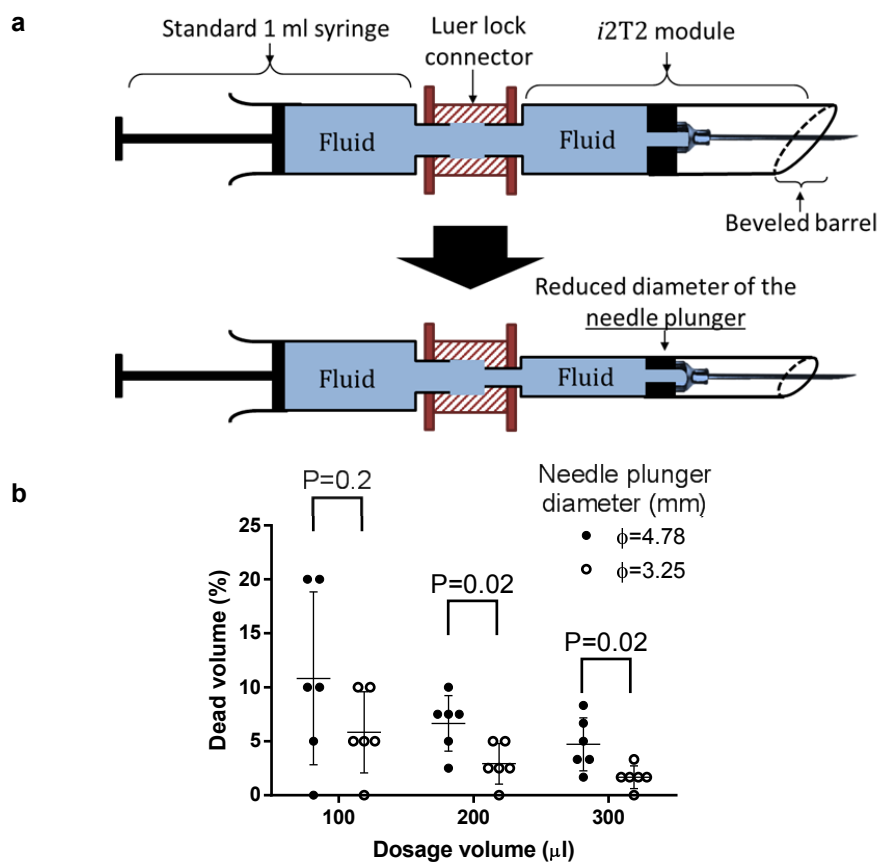
S4. Serial sections along the path of the needle targeting SCS



Supplementary figure S4: *i2T2* pierces through the sclera (a-r) to reach SCS and does not pierce the underlying layers. The needle hole in the sclera is indicated with an arrow. The undamaged RPE layer in sections (r-t) indicates that the needle did not pierce it. The retinal layers in certain sections were damaged during histological processing. (u) high magnification image of the region of interest showing needle entrance into the SCS. Choroid and sclera are separated by the injected fluid. The intact RPE shows that the needle did not penetrate deeper than the choroid. (v) high magnification image of the region past the

needle also shows the absence of RPE damage from the needle. The experiments were repeated independently (n=2) with similar results.

S5. Variability in dead volume can be reduced by decreasing the diameter of needle plunger



Supplementary figure S5: (a) *i2T2* can be easily modified to reduce the diameter of the needle plunger (b) Error introduced by dead volume within the *i2T2* is reduced by decreasing the diameter of needle plunger. Relative error also decreases with increasing dosage volume. (Number of independent measurements = 6. The error-bars indicate standard deviation. Two sided t-test results with a p-value of 0.2, 0.02, 0.02 for 100 μl , 200 μl , 300 μl respectively.)

S6. Use of *i2T2* in other tissue types and its potential applications

We have successfully tested the mechanism to travel through multiple types of tissues, including skin, muscle, and vessel wall to target cavities (or less dense tissue) below that tissue layer, towards a range of applications (subcutaneous fat injection, epidural injection, and vascular access (supplementary table-1)). Adjusting design parameters (fluid viscosity, internal friction, syringe and needle size) ensure use of optimal design for the given application. All the devices were assembled in-house using off-the-shelf components and tested on ex vivo tissue models. The table below lists the cavities of interest, tissue covering the cavity, specific model used for testing, *i2T2* design parameters and potential application.

Supplementary table 1

Potential applications	Tissue/cavity of interest	Tissue layer covering cavity/tissue of interest	Specific model	<i>i2T2</i> parameters		Advances through the tissue layer?	Automatic stop in the target
				Needle size	Syringe barrel		
SCS injections	Suprachoroidal space	Sclera	Bovine, porcine, rabbit eye globes	30 G	1 ml	✓	✓
Subcutaneous fat injections	Adipose tissue	Skin	Through porcine skin into underlying fat layer	30 G	1 ml	✓	✓
Vascular access	Vessel access	Vessel wall	Through porcine aorta wall into empty cavity	30 G	1 ml	✓	✓
Pediatric airway access	Airway	Connective tissue between cartilage rings and epithelial layer	Through space between tracheal rings (bovine) into the airway	26 G	3 ml	✓	✓
Intracardial injections	heart chamber	Heart wall	Through bovine heart wall into empty cavity	18 G*	20 ml	✓	✓
Laparoscopic surgery	Peritoneal cavity	Abdominal wall (skin, fat, muscle)	Through porcine belly into empty cavity	18 G*	20 ml	✓	✓
Epidural injections	Epidural space	Tissue above epidural space (skin, interspinous ligaments)	Through porcine back into empty spinal canal	18 G	20 ml	✓	✓

* The needle was modified to include a hydrogel plug to limit fluid flow within the tissue.

Supplementary video-1:

Ventricular access through heart wall using *i2T2* (*ex vivo* model)

Supplementary video-2:

Accessing peritoneal cavity through abdominal wall using *i2T2* (*ex vivo* model)